Journal of The Electrochemical Society

Model-Based Design of High Energy All-Solid-State Li Batteries with Hybrid Electrolytes

Journal of The Electrochemical Society, 2022 **169** 040550

Model-Based Design of High Energy All-Solid-State Li Batteries with Hybrid Electrolytes

Somayeh Toghyani,[1,*] Florian Baakes,[1] Ningxin Zhang,[2] Helmut Kühnelt,[2] Walter Cistjakov,[3,4] and Ulrike Krewer[1,4,z]

[1]*Karlsruhe Institute of Technology, Institute for Applied Materials-Electrochemical Technologies, 76131 Karlsruhe, Germany*
[2]*Center for Low-Emission Transport –Electric Drive Technologies AIT Austrian Institute of Technology GmbH, 1210 Vienna, Austria*
[3]*Institute of Energy and Process Systems Engineering, 38106 Braunschweig, Germany*
[4]*Cluster of Excellence SE[2]A-Sustainable and Energy-Efficient Aviation, Braunschweig, Germany*

As the aircraft industry becomes more committed to sustainable aviation, hybrid-electric propulsion systems containing batteries with higher gravimetric energy density attract increasing attention to reduce fuel consumption. Future aircrafts could benefit from next-generation chemistries like oxide-based all-solid-state Li-battery (ASSB) technologies. However, producing and evaluating a wide range of design parameters for maximising the gravimetric energy density of ASSB experimentally is both time- and resource-intensive. Physics-based modelling promises to identify optimal designs for battery cells with respect to high gravimetric energy density more time and cost-efficient. In this regard, we applied a pseudo-two-dimensional model for the model-based evaluation of Li-ASSB with various hybrid electrolytes containing oxide and polymer electrolytes. This way we elucidate which electrolyte performs well with present technology and which has the potential to become an attractive alternative in the future. After identifying design variables to improve ASSB with the help of sensitivity analysis, a genetic algorithm is used to predict the optimal design parameters to achieve higher gravimetric energy density. The conducted study reveals that ASSB based on 12.7 vol% of garnet $Li_{6.4}La_3Zr_{1.4}Ta_{0.6}O_{12}$ (LLZTO) is the best option based on present manufacturing constraints. Hybrid electrolytes based on 10 wt% of $Li_{1.3}Al_{0.3}Ti_{1.7}(PO_4)_3$ (LATP) could be promising for future aircrafts with further improvements in ASSB manufacturing process.

 [DOI: 10.1149/1945-7111/ac653b]

Manuscript submitted December 23, 2021; revised manuscript received March 8, 2022. Published April 25, 2022. *This paper is part of the JES Focus Issue on Women in Electrochemistry.*

Supplementary material for this article is available online

There is a growing interest in the sustainability of the aviation industry sector over the past years due to the environmental issues associated with traditional aviation engines. Electric and hybrid aircrafts are considered promising technologies for reducing fuel consumption and enhancing system efficiency.[1] However, in order to fulfil the high demands in this area, the electrical energy storage systems require a higher capacity-to-weight ratio[2] than today's Li-ion batteries. Another obstacle of Li-ion batteries with liquid electrolytes is the high flammability and the inherent thermal runaway risk.[3] Because of safety restrictions imposed by liquid electrolytes, which are more severe for Li-ion batteries with higher gravimetric energy density, such as Li-metal batteries, future development to obtain higher gravimetric energy density is impeded. These concerns motivate the development of next-generation chemistries, such as ASSB for aviation, which have non-flammable electrolytes.[4]

ASSB have been recently developed in various forms, such as solid polymer electrolyte-based (SPE), sulfide-based, halide-based, and oxide-based ASSB.[5,6] SPE and sulfide-based electrolytes have a narrow electrochemical potential window; as a result, their compatibility with high voltage cathode materials is limited.[7]

Oxide-based ASSB architectures have attracted continuing interest among researchers due to their relatively high ionic conductivity, ease of handling, and chemical stability in contact with Li metal and high cathode voltage materials. Recently, various kinds of oxide electrolytes, i.e., perovskite, NASICON, and garnet-type, have been widely studied. Perovskite, NASICON, and garnet-type oxide electrolytes have all lately been studied extensively.[6] Perovskite electrolyte of $Li_{0.05-3x}La_{0.5+x}TiO_3$ (LLTO) has a crystal structure; its instability in contact with Li, and high grain boundary resistance limit its use in practical applications. However, such electrolytes have interesting features such as high electrochemical stability and stability in moist atmospheres.[8] Na-based superionic conductors (NASICON) have also a crystal structure, and they are brittle because of their intrinsic nature. However, the hexagonal-type structures of LATP and $Li_{1.5}Al_{0.5}Ge_{1.5}P_3O_{12}$ (LAGP) were well studied among NASICON electrolytes because of their high ionic conductivity. LATP undergoes the reduction of Ti^{4+} to Ti^{3+} when exposes to lithium, which results in forming an ionic and electronic mixed conductive interface and induces cell instability. However, researchers are interested in developing such electrolytes and improving their stability in contact with lithium to build a cell with higher gravimetric energy density due to their low density. LAGP are less vulnerable to phase transitions and have high stability in the air environment. LAGP has often been stated in the literature that it's relatively stable in contact with lithium.[9] Garnet structured electrolytes have a wide electrochemical window and are stable against lithium; they could be a promising option for ASSB using Li metal anode. However, at room temperature, the tetragonal phase of LLZO with low conductivity is more stable than its cubic phase with higher conductivity. Incorporating doping elements with tantalum (Ta) within the garnet crystalline structure could stabilise the cubic garnet structure of LLZTO at low temperatures.[10]

The major drawbacks associated with oxide-based solid electrolytes are weak contact between electrode and electrolyte interface, low mechanical flexibility, and high density i.e. weight. These issues limit their use for high gravimetric energy density applications.[11] To mitigate the aforementioned concerns, the solid polymer composite electrolytes (SPCE) approach is applied, where oxides are mixed with polymer electrolytes.[12] In this regard, many researchers have widely utilised poly (ethylene oxide) (PEO), lithium bis (fluorosulfonyl)imide (LiTFSI), poly (propylene carbonate) (PPC), and a combination of them with oxide-based solid-state battery architectures.[8] The crystallinity of PEO could be significantly

*Electrochemical Society Member.
[z]E-mail: ulrike.krewer@kit.edu

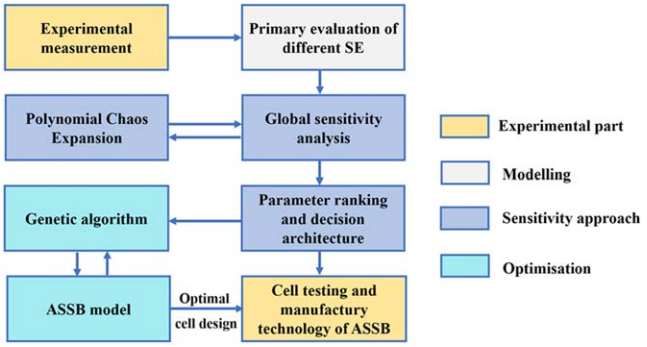

Figure 1. Pathway overview of model-based optimisation of ASSB.

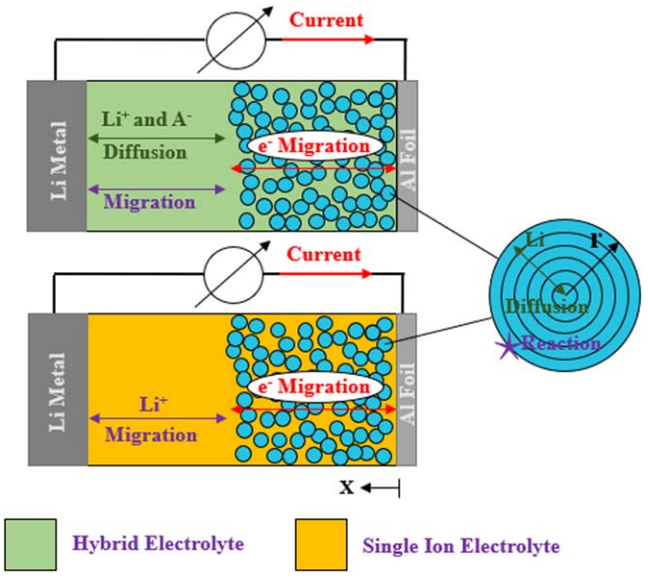

Figure 2. Schematic representation of Li/NMC for a single cell of Li-ASSB with SIC and hybrid electrolytes.

decreased by adding poly (propylene carbonate) (PPC) to the PEO matrix. Additionally, some electrochemical properties, such as electrochemical stability window and ionic conductivity, as well as some mechanical properties, could be enhanced.[13] Also, ionic liquids are seen as an interesting alternative to PEO, as they are still flexible, have a wider electrochemical window, have better chemical stability, and show higher conductivities; therefore, the mixtures with polymerised ionic liquid (PIL) instead of PEO could be interesting electrolyte for ASSB.[9]

So far, several studies have experimentally investigated the electrochemical characteristics, the electrochemical stability window of hybrid electrolytes as well as their compatibility with Li metal. Furthermore, most previous studies have focused on reducing the contact resistance between electrodes and electrolyte in ASSB, improving ionic conductivity of ASSB, and suppressing Li dendrite growth in contact with Li. High ionic conductivity and diffusivity are important for thick electrodes to reach a high energy density at a high discharge rate. However, designing an optimum cell without ion transport limitations in such cells using experimental investigations is time- as well as resource-intensive due to the large number of iterations in production and evaluation required to achieve a well-performing design. Physics-based modelling aims to create a platform that can directly assess the impact of cell structure on battery performance and provide knowledge concerning limiting processes within the cell. Therefore, modelling promises to identify optimal cell designs for battery cells with respect to the high gravimetric energy density in a more time- and cost-efficient way.

To find the optimal design of ASSB using parametric studies, a large number of simulations is required; additionally, gradient-based approaches tend to become stuck in a local minimum, and their performance is influenced by the starting value of design variables. To avoid the probability of being stuck at a local optimum point, genetic algorithms (GA) should be applied, which will find an optimal solution through searching a series of points rather than a single point.[14] However, a large number of decision variables results in a broad and complicated search space, which is one difficulty that needs to be addressed in the GA application. As a consequence, before implementing GA, it is essential to understand which battery factors have a substantial impact on battery performance. Similarly, as for Li-ion batteries,[15,16] integration of sensitivity analysis and physics-based modelling could provide a thorough knowledge for ASSB and aid in selecting appropriate GA decision criteria.

Few studies have been carried out on the modelling of single ion conductor (SIC) electrolytes with physics-based modelling. Becker-Steinberger et al.[17] implemented a one-dimensional (1D) model to simulate the discharge curve of the cell with SIC electrolyte. They examined the double layer at the electrolyte/solid interface. Further, our group[18] compared the cell performance of binary liquid electrolyte and SIC electrolyte using a pseudo-two-dimensional (P2D) model. We demonstrated the sensitivity of both systems to electrode thickness and electrolyte conductivity. In another study, Danilove et al.[19] simulated the performance of the SIC electrolyte using a 1D model. Their model provides extensive information such as concentration profiles, migration flows, and overpotential contributions throughout the electrolyte. Laue et al.[20] employed a three-dimensional microstructure model to simulate the impact of mixing methods on microstructural features of the solid-state electrode. Their model examined the effect of microstructure characteristics and electrode composition on effective electronic and ionic conductivities, as well as the electrochemical active area. Surrogate models of such microstructure models then allow to integrate effective microstructure models in P2D battery models.[21]

Previous numerical models focused on the SIC electrolyte and did not consider solid-state hybrid electrolytes as a way to address SIC electrolyte concerns such as low energy density, insufficient flexibility, and poor contact between electrode and electrolyte interface. We here present the first study that combines an ASSB model and a wide range of (hybrid) electrolytes with an evolutionary algorithm to identify optimum cell designs to reach a higher gravimetric energy density. To this end, we first compare the performance of several hybrid electrolytes of oxide and polymer with their experimental properties, to suggest the best solid electrolyte (SE) in terms of gravimetric energy density. Following that, a sensitivity analysis of the battery cell is performed on the identified electrolyte to discover which battery parameters have the most influence on the battery performance. The findings of the sensitivity analysis will subsequently be utilised to select decision factors for the ASSB model's optimisation. Then, this model is incorporated into the GA to find the optimal cell design. Finally, recommendations are derived after comparing both primary and optimal cell designs. A pathway overview of our study is depicted in Fig. 1.

Methodology

Simulation methodology.—The area of battery modelling is vast, with several available models for selection. These models differ in terms of complexity, reliability, and computational cost. The three most common battery models are data-driven models, equivalent circuit models, and mechanistic models. Mechanistic models are based on chemical and physical knowledge and aim to interpret the processes that take place within or between the components, which affect the battery performance.[22] The P2D model is the most common mechanistic model for single cells, which was developed by Doyle et al.[23] P2D models make it possible to examine a wide range of variations in geometric, material, and operating parameters with a relatively low computational effort by employing the porous

Table I. Summary of hypothesis for Li-ASSB with SIC and SPCE electrolytes [18].

Assumptions
• Both solid and electrolyte phases have isotropic characteristics.
• The porous electrodes are modelled as a homogenous geometry with uniform spherical particles.
• The cell operates at a constant temperature of 60 °C.
• There are no side reactions between the electrode and electrolyte.
• Ideal contacts are assumed for all contact areas.
• Only migration processes inside the composite cathode and SIC electrolyte are simulated.[a)]
• Migration and diffusion phenomena within the composite cathode and SPCE electrolyte are modelled.
• Li transfer number (t_p) of SIC electrolyte is equal to one and t_p for SPCE electrolyte is defined based on existing experimental data in Table II.
• No concentration gradient exists inside the SIC electrolyte as the negative counter ion is locally fixed, but there is a concentration gradient within the SPCE electrolyte
• The lithium foil is modelled as a boundary condition.

a) We assume a reversible Li metal anode with fast reactions and negligible transport effects in the electrode. Thus, we only simulate migration processes inside the composite cathode and SIC electrolyte separator.

electrode theory. The P2D model framework is based on diffusion, migration, Li-ion accumulation as well as electrical charge in the direction of electrode thickness, diffusion, and Li accumulation in a radial dimension inside active material particles, and reaction kinetics at the interface of active material and electrolyte. In the present study, we employ a P2D model to simulate the electrochemical performance of Li-ASSB with SIC and SPCE electrolytes, as illustrated in Fig. 2.

The single cell comprises Li metal as the anode side, SIC and SPCE electrolytes, and the cathode, which is composed of NMC811 active material and SE. Table I summarises the primary hypotheses for the implementation of the Li-ASSB model.

In contrast with the classical P2D model, the equations for calculating electrolyte potential and concentration of SIC are according to the work of Wolff et al.[18] In his modelling, diffusion and convection processes within the electrolyte phase were ignored. For modelling of Li-ASSB with SPCE electrolyte, we considered the diffusion and migration processes inside the electrolyte phase; because there is Li salt inside the polymer-based electrolyte, and both anion and cation are mobile in hybrid electrolytes.[18] The electrolyte potential and concertation of SPCE electrolytes are determined based on the classical P2D equations. However, due to a lack of experimental knowledge, we did not take into account the dependency of the ionic conductivity of hybrid electrolytes and electrolyte diffusion coefficient on electrolyte concentration. Instead, we introduced a constant value of ionic conductivity at a specific temperature based on experimental data; because the ionic conductivity of the SPCE electrolyte is strongly dependent on temperature. Then the Einstein relation is used to calculate the electrolyte diffusion coefficient, D_e, from the ionic conductivity of SPCE electrolyte, σ_e.[30]

$$D_e = \frac{\sigma_e R\, T}{F^2 z^2 c_e} \quad [1]$$

where, c_e is the Li concentration in the electrolyte phase, F is the Faraday constant, R is the universal gas constant, T is temperature, and z is the charge number.

Table III illustrates the governing equation of the physicochemical P2D model, which is applied to model Li-ASSB with SIC and SPCE electrolytes. The principal characteristics of these equations are listed as follows. Eqs 2 and 3 indicate the electrolyte phase potential, ϕ_e, which is computed using Kirchhoff's and Ohm's laws for SPCE and SIC electrolytes, respectively. The effective ionic conductivity, $\sigma_{e,eff}$, within the electrolyte phase, is derived using the relation between the Bruggeman coefficient, β, and tortuosity, τ, as given in Eqs. 4 and 5. The charge balance in the electrode phase, ϕs, is governed by Ohm's law as written in Eq. 6. The effective solid-phase conductivity is estimated using Eq. 7. Total and double layer Li current density can be determined using Eqs. 8 and 9, respectively. The concentration of Li-ions in the electrolyte phase for Li-ASSB with SPCE and SIC electrolytes, is described by Eqs. 10 and 11 respectively.[31] As indicated in Eq. 12, the effective electrolyte diffusion coefficient is calculated by applying the Bruggeman factor. The solid phase concentration, c_s, in the spherical particles is defined based on Fick's law using Eq. 13. The charge transfer reaction at the interface of the solid phase and electrolyte phase is described by Butler-Volmer kinetics, as given in Eq. 14. In this equation, a_s is the specific surface area of the cathode active material that is in contact with the electrolyte. Assuming spherical particles, it is calculated by Eq. 15. The exchange current density, i_0, in the Butler-Volmer equation is dependent on the concentration of electrolyte at the electrode/electrolyte interface and the kinetic rate constant, k, and can be determined by Eq. 16. The cell overpotential is expressed as the deviation between the state-of-charge (SOC)-dependent open-circuit voltage (OCV), U_0, and the potential difference between the electrolyte and solid phase and can be calculated using Eq. 17. In the present study, the dependence of OCV on SOC is based on our measurements as a starting point for all simulations, as described in Table SI.

The gravimetric energy density, E_G, can be computed by dividing the integral of instantaneous power from 0 to time to reach the cut-off voltage ($t_{cut-off}$) by the mass of the cell (Eq. 18). For estimating the mass of the cell, M_{cell}, the mass of the current collectors, anode and cathode electrodes, and solid electrolytes are considered (Eq. 19). The volumetric energy density is also estimated by dividing cell energy by the volume of the cell, V_{cell}, as described in Eqs. 20 and 21.

$$E_G = \frac{\int_0^{t_{cutoff}} U_{cell}\, I\, dt}{M_{cell}} \quad [18]$$

$$M = (\delta_{ac}\rho_{ac}A_{ac} + \delta_{SE}\rho_{SE}A_{SE} + \delta_c\rho_c\varepsilon_s A_c + \delta_c\rho_e\varepsilon_e A_c + \delta_a\rho_a A_a + \delta_{cc}\rho_{cc}A_{cc}) \quad [19]$$

$$E_V = \frac{\int_0^{t_{cutoff}} U_{cell}\, I\, dt}{V_{cell}} \quad [20]$$

$$V_{cell} = (\delta_{ac}A_{ac} + \delta_{SE}A_{SE} + \delta_c\varepsilon_s A_c + \delta_c\varepsilon_e A_c + \delta_a A_a + \delta_{cc}A_{Cc}) \quad [21]$$

where, A_{ac}, A_{cc}, A_{SE}, A_a, and A_c are the geometrical area of the anode and cathode current collectors, solid electrolyte, and the anode and cathode electrodes, respectively. They can be calculated using diameters, which are listed in Table IV. MATLAB 2019b has been used to conduct all simulations with the ASSB model. The finite volume method is applied for spatial discretisation of partial differential equations, and ODE15 solver solves the time derivatives. Discretisation for all simulations in this paper was carried out in two directions: x-direction for the electrode and solid electrolyte layer with computational domains of 10 each, and r-direction from particle center to particle surface with 10 computational domains.

Parameterisation and experimental section.—Since the goal of this study is to anticipate ASSB with potentially high performance in the aviation industry, we employ NMC811 as the cathode and Li

metal as the anode in our simulation to achieve a higher gravimetric energy density. However, as is typical with manufacturing of new battery technologies, the cell with the mentioned chemistry didn't experimentally work properly, especially at higher current rates. Because of this, we used the cell containing NMC622 and graphite, which we experimentally constructed, to show that our model is able to reproduce ASSB cells at the example of an ASSB containing NMC622 (see Fig. S1 (available online at stacks.iop.org/JES/169/040550/mmedia)). As we did not get a set of experimental results for a proper parameterisation of the NMC811 chemistry we assumed similarity between NMC622 and NMC811 reaction kinetics. It should be noted that the identical hybrid electrolyte was utilised for both cells. Furthermore, for cells with NMC622 and NMC811, the same thickness of cathode and anode electrodes, as well as the solid electrolyte, were used. However, we didn't use the cell with NMC622 and graphite for the simulation because the practical capacity gained was insufficient for usage in the aviation industry. Since the results of a parametric study on the ASSB based on Li metal anode and NMC811 motivate further development in the cell structure of ASSB and could provide information concerning limiting processes within the cell, we used this type of cell in our investigation. The geometrical features of the battery, along with physical and electrochemical properties, are given in Table IV. We extracted the following cell and electrode parameters from our cells with Li and NMC811 electrodes: particle size, cell geometry, Li diffusivity in the active material, the volume fraction of active materials, the thickness of the anode and cathode electrodes, and NMC811 open-circuit voltage. Reaction kinetic constants were adapted from NMC622, as they require an experimentally working cell (see above). For comparative analysis of a wide range of electrolytes, we exclusively used typical electrolyte parameters from literature, e.g. the typical thickness, ionic conductivity, and t_p of a given hybrid electrolyte It should be mentioned that the nonlinear dependence of t_p on the mass fraction of a given electrolyte is implemented in the simulation, which is based on reported experimental data in Table II. In the following, the manufacturing of the Li/NMC811 electrodes and the cell setup of the mentioned cell will be described.

Raw materials.—The raw materials for the preparation of hybrid solid electrolyte films are all pre-treated to remove absorbed humidity in vacuum and at certain temperatures. PEO (m.w. 600,000, Acros, Germany) powder was dried at 55 °C in vacuum for 12 h, and then stored in the dry room, LICGC (Li-ion conductive glass ceramics, Ohara Inc., Germany) and LLZO (NEI Corp., USA) powders and LiTFSI powder were dried at 120 °C in vacuum for 12 h and stored in the dry room. Acetonitrile (Sigma-Aldrich, Germany) was used as solvent.

NMC811 powder (Targary Ltd., USA) and Carbon black C65 (Imerys, Switzerland) powders are all kept in an oven set at 100 °C before use, and PVDF powder (Solvay, France) was used as it was received. NMP was used as solvent.

Preparation of hybrid solid electrolyte films.—For the preparation of hybrid solid electrolyte films, LiTFSI powder and oxide electrolyte powder (LICGC and LLZO) were weighed and added to a certain amount of acetonitrile, and mixed for 30 min vigorously, then the dispersion was ultrasonically treated for 1 h. Then PEO powder was added to the as-received dispersion during mixing to facilitate the dissolution of PEO. The concentration of PEO is around 8 wt%. After mixing overnight, the white homogenous dispersion was sealed tightly and ultrasonically treated for 1 h again, and slowly mixed for 30 min to remove bubbles from the slurry of the hybrid solid electrolyte.

Doctor blade coating was performed to prepare films of hybrid solid electrolyte, a gap of 1250 mm was chosen with a coating speed of 4 mm s^{-1}. To facilitate the drying process, a PTFE film (0.5 mm in thickness reinforced by glass fibers) was adhered to a pentax substrate to match the stress between the dried solid electrolyte film and the pentax substrate. The wet film was naturally dried in air for 4 h, then sent to a vacuum oven and dried at 100 °C in vacuum for 16 h. All the experiment except ultrasonic treatment was performed at a dry room with a dewing point no higher than −40.0 °C.

The dried hybrid solid electrolyte films were released from the substrate carefully and can stand by themselves, they were cut punched into circles for assembly of coin cells.

Preparation of cathode.—For the preparation of the cathode, PVDF powder was firstly dissolved into NMP overnight to form a PVDF solution of ∼8 wt%, then C65 and active material powder (NMC811) were added to the PVDF solution. The kneading process was used to mix solid powders (C65 and NMC811) in PVDF solution to form a homogenous slurry of NMC811. The slurry was mixed then overnight and coated on Al foil with a gap of 120 μm. After natural drying of wet NMC811, it was dried in a vacuum oven at 120 °C for 16 h. The dried NMC811 electrodes were punched into circles with a diameter of 15 mm. The cut circle cathodes were dried at 100 °C in vacuum for 16 h, then transported to a glove box filled with argon gas to keep the content of oxygen and water both around 1 ppm.

Assembly of all-solid-state CR2016 coin cells.—Assembly of CR2016 coin cells was performed in a glove box, Li metal ribbons with a diameter of 16 mm and 70 μm in thickness are used as the anode. A hybrid solid electrolyte film is used to suppress the growth of Li dendrites during the electrochemical process. Symmetric cells with stainless steel pieces as Li-blocking electrodes were also assembled, where hybrid solid electrolyte film was sandwiched between stainless steel electrodes. Fig. S2 shows the SEM images of the surface morphology and cross-section view of LATP based hybrid solid electrolyte as well as NMC811. This figure shows the homogeneous distribution of oxide-based electrolyte in the hybrid electrolyte, which is required to achieve high performance of ASSB. The SEM pictures are used to show that the hybrid electrolyte works and is microscopically distributed. Since the surface and cross-section of the hybrid electrolyte film had no obvious porous structure, therefore the homogeneous mixtures, which we consider for the modelling of ASSB could be a suitable approach.

Sensitivity analysis.—The ability to measure the individual and common influences of the parameters on the performance of ASSB can be provided by sensitivity analysis. This knowledge is helpful for cell testing, the manufacturing technology of ASSB, and battery management systems.[16] This approach could significantly reduce the need for extensive experimental studies of several variables by providing adequate quantitative information about parameter ranking. It is also essential for choosing decision variables of the battery model optimisation.

There are two methods for sensitive analysis, local and global. Sensitivity analysis in the local approach is defined around a single operating point in parameter space. This approach is highly dependent on parameter space position and ignores critical parameter interactions. While in the global strategy, the analysis will be performed across a given domain in parameter space. It also examines the individual and combined effects of parameter variation and quantifies model response variance across the entire parameter domain. Hence, we here apply global sensitivity analysis to determine the most influencing variables on the gravimetric energy density of the ASSB.[35]

In order to estimate the sensitivity indices, we apply the variance-based global sensitivity approach, also known as the Sobol approach, which already proved suitable for analysing Li-ion batteries.[16] This approach is based on the decomposition of the variance of the model output into the summand of variance of individual or interaction of input parameters. The Sobol sensitivity indices estimate how much each input factor contributes to the variation of the model output. When a parameter has a low sensitivity index this results in small changes in the final model output. If a parameter has a high

Table II. Li-ion transfer number, ionic conductivity, and thickness of hybrid solid electrolytes of oxides and polymers as reported in the literature.

Electrolyte type	Group type	Li-ion transfer number (t_p)	Ionic conductivity, S cm^{-1}	Thickness of SE layer, μm
PEO-LiTFSI[8]	Polymer	0.15	2.65×10^{-4}	130–150
PEO-PPC- LiTFSI[13]	Polymer	0.177	2.71×10^{-4}	130–150
PEO-PPC- LiTFSI/LLTO (8 wt%)[13]	SPCE based on perovskite	0.227	4.72×10^{-4}	135
PEO- LiTFSI/LLTO (5 wt%)[8]	SPCE based on perovskite	0.195	3.63×10^{-4}	135
PEO- LiTFSI /LLZTO (5.2 vol%)[10]	SPCE based on garnet	0.31	2.31×10^{-4}	40
PEO- LiTFSI /LLZTO (8.6 vol%)[10]	SPCE based on garnet	0.37	3.05×10^{-4}	40
PEO- LiTFSI /LLZTO (10.5 vol%)[10]	SPCE based on garnet	0.42	4.65×10^{-4}	40
PEO- LiTFSI /LLZTO (12.7 vol%)[10]	SPCE based on garnet	0.46	5.63×10^{-4}	40
PEO- LiTFSI /LLZTO (15.1 vol%)[10]	SPCE based on garnet	0.43	5.07×10^{-4}	40
PEO- LiTFSI /LLZTO (17.9 vol%)[10]	SPCE based on garnet	0.39	4.72×10^{-4}	40
PEO- LiTFSI /LLZTO (21.1 vol%)[10]	SPCE based on garnet	0.33	3.68×10^{-4}	40
PIL-LiTFSI[9]	Polymer	0.07	4.84×10^{-4}	200
PIL-LiTFSI/LATP (10 wt%)[9]	SPCE based on NASICON	0.21	5.92×10^{-4}	200
PIL-LiTFSI/LATP (20 wt%)[9]	SPCE based on NASICON	0.15	4.09×10^{-4}	200
PIL-LiTFSI/LATP (30 wt%)[9]	SPCE based on NASICON	0.12	3.5×10^{-4}	200
PIL-LiTFSI/LATP (40 wt%)[9]	SPCE based on NASICON	0.09	3.06×10^{-4}	200
PEO- LiTFSI/LAGP (20 wt%)[12]	SPCE based on NASICON	0.168	2.94×10^{-4}	200
PEO- LiTFSI/LAGP (40 wt%)[12]	SPCE based on NASICON	0.175	5.17×10^{-4}	200
PEO- LiTFSI/LAGP (60 wt%)[12]	SPCE based on NASICON	0.213	5.8×10^{-4}	200
LLZO[24]	SIC based on garnet	1	8.41×10^{-3}	300
LLZTO[24]	SIC based on garnet	1	9.54×10^{-3}	300
LLTO[25]	SIC based on perovskite	1	5.27×10^{-3}	300
LATP[26–28]	SIC based on NASICON	1	5×10^{-3}	300
LAGP[29]	SIC based on NASICON	1	1.35×10^{-3}	300

Table III. Governing equation of physicochemical model for Li-ASSB with SIC and SPCE electrolytes.

	Charge balance in the electrolyte phase		
$\sigma_{e,eff}\frac{\partial\phi_e}{\partial x}+2\frac{RT}{F}\sigma_{e,eff}\left(t_p-\frac{1}{2}\right)\frac{\partial ln\ c_e}{\partial x}=-J$	SPCE	[2]	BC: $\phi_e(0)=0\frac{\partial\phi_e(L)}{\partial x}=0$
$\sigma_{e,eff}\frac{\partial\phi_e}{\partial x}=-J$	SIC	[3]	
$\sigma_{e,eff}=\frac{\varepsilon_e}{\tau}\sigma_e$		[4]	
$\tau=\varepsilon_e^{1-\beta}$		[5]	
	Charge balance in the electrode phase		
$\frac{\partial}{\partial x}\left(\sigma_{s,eff}\frac{\partial\phi_s}{\partial x}\right)=j_{tot}$		[6]	BC: $\frac{\partial\phi_s(0)}{\partial x}=-\frac{\partial\phi_s(L)}{\partial x}=\frac{I}{A\sigma_{s,eff}}$
$\sigma_{s,eff}=\varepsilon_s\ \sigma_s$		[7]	
$j_{tot}=j_{Li}+j_{DL}$		[8]	
$j_{DL}=a_sC_{DL}\frac{\partial(\phi_s-\phi_e)}{\partial t}$		[9]	
	Mass conservation in the electrolyte phase		
$\varepsilon_e\frac{\partial c_e}{\partial t}=D_{e,eff}\frac{\partial^2c_e}{\partial x^2}+(1-t_p)\frac{j_{Li}}{F}$	SPCE	[10]	BC: $\frac{\partial c_e(0)}{\partial x}=0\ \frac{\partial c_e(L)}{\partial x}=-\frac{I(1-t_p)}{FD_{e,eff}}$
$\frac{\partial c_e}{\partial t}=0$ SIC		[11]	
$D_{e,eff}=\frac{\varepsilon_e}{\tau}D_e$		[12]	
	Mass conservation in electrode phase		
$\frac{\partial c_s(r)}{\partial t}=\frac{1}{r^2}\frac{\partial}{\partial r}\left(D_sr^2\frac{\partial c_s(r)}{\partial r}\right)$		[13]	BC: $\frac{\partial c_s(0)}{\partial r}=0\ \frac{\partial c_s(R)}{\partial r}=\frac{j_{Li}}{a_sF}$
	Electrochemical reaction		
$j_{Li}=a_si_0\left(\exp\left(\alpha\frac{\eta F}{RT}\right)-\exp\left(-(1-\alpha)\frac{\eta F}{RT}\right)\right.$		[14]	
$a_s=3\frac{\varepsilon_{s,i}}{R_i}$		[15]	
$i_0=kFC_e^{\alpha}(c_{s,\max}-c_s)^{\alpha}\ {c_s}^{1-\alpha}$		[16]	
$\eta=\phi_s-\phi_e-U_0$		[17]	

sensitivity index, changing it causes the model output to change drastically.[36] Here we present a brief description of the Sobol index. Assuming a defined model, such as $Y=f(X)$, where Y is the model output and $X(x_1, x_2,\ldots x_n)$ are the input parameter vectors. The total output variance of output Y, which is the summand of the partial variances can be calculated by Eq. 22:[37]

$$V(Y)=\sum_{i=1}^{n}V_i+\sum_{i\leqslant j\leqslant n}^{n}V_{ij}+\ldots+V_{i,\ldots,n} \quad [22]$$

The total variance is used to normalise these partial variances. The first order Sobol index, which represents the influence of a single input parameter on the model output, can be determined as the ratio of partial variance to the total variance. In contrast, the higher order of the Sobol index indicates the impact of input parameter interaction on the output results.

$$S_i=\frac{V_i}{V}\quad \text{First-order Sobol index} \quad [23]$$

$$S_{ij}=\frac{V_{ij}}{V}\quad \text{Second-order Sobol index} \quad [24]$$

The total sensitivity index or total effect of each input parameter can be defined as a sum of all orders of sensitivity index as Eq. 25, which considers both, first and second orders as well as higher order effects for the comprehensive evaluation over the whole parameter space:[37]

$$S_T=S_i+\sum_{i\neq j}S_{ij}+\ldots \quad [25]$$

The Sobol index can be computed using a variety of methods. In the present study, the polynomial chaos expansion method for sensitivity analysis is applied due to its effectiveness concerning computational time.[16] As listed in Table V, for the uniform distribution, a lower and upper boundary of parameters is required. We utilised the Bruggeman factor to estimate tortuosity based on Eq. 5. Based on our knowledge, this boundary was not available in literature data for the Bruggeman coefficient in solid-state batteries. For this reason, we considered the Bruggeman factor of 1.5 for perfect spheres as a mean value for the Gaussian distribution with a standard deviation of 10%.[34] The considered input parameters of the present study for the sensitivity analysis are Li transfer number, the thickness of cathode and electrolyte, particle size of cathode material, volume fraction of cathode material, the electronic conductivity of active material, and tortuosity. The gravimetric energy density is considered as the output variable. When the Sobol index is close to zero, it indicates that the parameter does not influence the output variable. Sobol index close to one denotes that the parameter has a significant impact on the output variable.[38]

Optimisation.—In general, an optimisation problem is defined as following:[42]

$$\text{minimise f(x)}\quad \text{subject to}\begin{cases}\mathrm{x_{lower\ bound}}\leqslant & \mathrm{x}\leqslant\mathrm{x_{upper\ bound}}\\ \mathrm{c_k(x)}\leqslant 0 & \mathrm{k=1,\ldots,m}\\ \mathrm{c_i(x)}=0 & \mathrm{i=1,\ldots,n}\end{cases} \quad [26]$$

where f(x) is the objective function that should be minimised under the equality and inequality constraints, $c_i(x)$ and $c_k(x)$, respectively. In the current study, negative gravimetric energy density is the objective function, and decision variables for the optimisation will be selected based on provided results by sensitivity analysis.

Various mathematical methodologies have been used to deal with optimisation problems, such as classical methods and evolutionary algorithms. A classical approach like gradient-based methods is known to generate outstanding results in a short time, but they are prone to be stuck in the local optimum point. The classical approach does not function well over a wide diversity of problem domains, and they are inefficient when the search space is too broad. To avoid

Table IV. Geometry data and physical and electrochemical features of the single cell.

Parameter	Symbol	Value
Geometry data		
Thickness of anode/cathode, μm	δ_a/δ_c	70/55
Thickness of anode/cathode current collector, μm	δ_{ac}/δ_{cc}	0/15
Diameter of anode/cathode/SE layer of coin cell, cm	$D_a/D_c/D_{SE}$	1.6/1.5/1.9
Diameter of anode/cathode current collector layer of coin cell, cm	D_{ac}/D_{cc}	1.5
Volume fraction of active material	ε_s	0.44
Volume fraction of electrolyte	ε_e	0.327
Particle size, μm	R	5.85
Physical and electrochemical properties		
Temperature, °C	T	60
Faraday Constant, C mol^{-1}	F	96485
universal gas constant, J mol^{-1} K^{-1}	R	8.314
Lithium transfer number	t_p	Table II
Density of NMC811/, kg m^{-3} [32]	ρ_c	4870
Density of SE, kg m^{-3}	ρ_{SE}	Fig. 3a
Density of Li, kg m^{-3} [33]	ρ_a	534
Density of cathode current collector, kg m^{-3}	ρ_{cc}	2700
Electronic conductivity of NMC, S m^{-1} [32]	σ_s	0.17
Electrolyte phase ionic conductivity, S m^{-1}	σ_e	Table II
Li diffusivity in active material, m^2 s^{-1} [own measurements]	D_s	4.84×10^{-14}
Electrolyte diffusion coefficient, m^2 s^{-1}	D_e	Table II and Eq. 1
Maximum solid phase concentration, mol m^{-3} [32]	$c_{s,\,max}$	50060
Initial electrolyte concentration, mol m^{-3} [16]	$c_{e,0}$	1200
Charge transfer coefficient	α	0.5
Double-layer capacitance at cathode/electrolyte interface, Fm^{-2} [34]	C_{DL}	0.2
Tortuosity	τ	Eq. 5
Bruggeman coefficient[34]	β	1.5
Open circuit voltage, V	U_0	Table SI

the probability of being stuck at a local optimum point, a genetic algorithm has been applied. This algorithm is an appropriate strategy for multi-dimensional and nonlinear systems, which search a series of points rather than a single point. This approach offers a simple way to come up with a feasible solution with no continuous derivative and various constraints.[43]

GA process begins with a random set of solutions to explore the solution space of the problem. The efficiency of each solution is assessed using a fitness value that is based on the objective function. This procedure is followed by examining the optimum solution, i.e., whether all of the explored solutions are attained to an optimal level of fitness or not. If not, some of the current generation, based on its fitness value, is selected as a parent. Here, the Roulette Wheel method is applied to choose the parent generation. Using the crossover and mutation operators, the children generation generates and substitutes with the existing generation.[44] The new solution set will be once again examined. If the stopping condition is met, the algorithm will be terminated; otherwise, the procedure will be repeated until one of the stopping conditions is fulfilled.

To utilise this strategy, it is necessary to first specify decision variables, their constraints, and an objective function, as well as identify the number of generations, population size, and general options. The crossover and mutation rates, population size, and generation number are chosen 0.8, 0.1, 100, and 80, respectively, in the present study.

Results

This section starts with evaluating the performance of various SIC electrolytes and hybrid electrolytes of oxide and polymer to identify the best solid electrolyte in terms of gravimetric energy density with current technology as well as the most promising electrolyte composition for the future. Then, the sensitivity analysis is carried out on the proposed best electrolyte to specify which battery parameters have the most considerable impact on the gravimetric energy density. Thenceforth, sensitivity analysis results will be employed to select decision factors for the optimisation of the battery model. In the next step, we apply a global optimisation

Table V. List of input parameters in the sensitivity analysis of ASSB.

Variable name	Minimum	Maximum	Distribution type
Li transfer number, t_p (Table II)	0.15	0.46	Uniform
Cathode thickness, δ_c (μm)	40	80	Uniform
SE thickness, δ_{SE} (μm)	40	100	Uniform
Cathode particle radius, R (μm)[39]	3	13	Uniform
Volume fraction of active material, ε_s[40]	0.4	0.65	Uniform
Electric conductivity, σ_s (Sm^{-1})[41]	0.01	1	Uniform
	Expected value	**Standard deviation**	**Distribution type**
Bruggeman factor, β[34]	1.5	10%	Gaussian

Table VI. Comparison of reference and optimum solid-state battery design for a cell with 12.7 vol% LLZTO, Li metal as the anode, and NMC811 as cathode at two current rates. Further parameters see Tables II, IV, and SI.

	δ_{cat} (µm)	ε_s	Gravimetric energy density, Wh kg^{-1}	Volumetric energy density, Wh L^{-1}	Average power density, W kg^{-1}
Reference design, 0.1C	55	0.44	410.7	813	42.12
Optimal design for 0.1C	77	0.63	618	1251	63.81
Optimised cell for 0.1C, discharge at 1C	77	0.63	73.66	149.15	628.99
Reference design 1C	55	0.44	341.66	676.62	400.91
Optimal design for 1C	43	0.48	351.36	721.71	385.34
Optimised cell for 1C, discharge at 0.1C	43	0.48	395.44	812.26	39.61

algorithm to find an optimum design of the battery cell based on suggested decision variables by sensitivities analysis. Eventually, both primary and optimal electrode designs are compared at different current rates, and recommendations are inferred.

A comparative study of various SIC and hybrid electrolytes of oxide and polymer.—Here, we first examine with the proposed model the performance of several types of SPCE electrolytes with different percentages of inorganic oxides-based electrolytes. As not every electrolyte can presently be manufactured in thin layers, experimentally reported thicknesses of solid electrolytes for each group of electrolytes are considered, as detailed in Table II. The best-performing electrolytes among various groups of oxide electrolytes, i.e., perovskite, garnet, and NASICON, and hybrid electrolytes are then identified. Furthermore, the compatibility with Li and the high voltage cathode should be taken into account when choosing the best electrolyte type; the selected electrolyte should be stable up to 4.5 V because the operating window of NMC811 is up to 4.5 V.[45]

Figures 3b and 3c show a performance comparison of oxide-based SPCE electrolytes in terms of practical gravimetric energy density at two discharge rates. It is assumed that all cells have the same anode and cathode electrodes. The only difference between

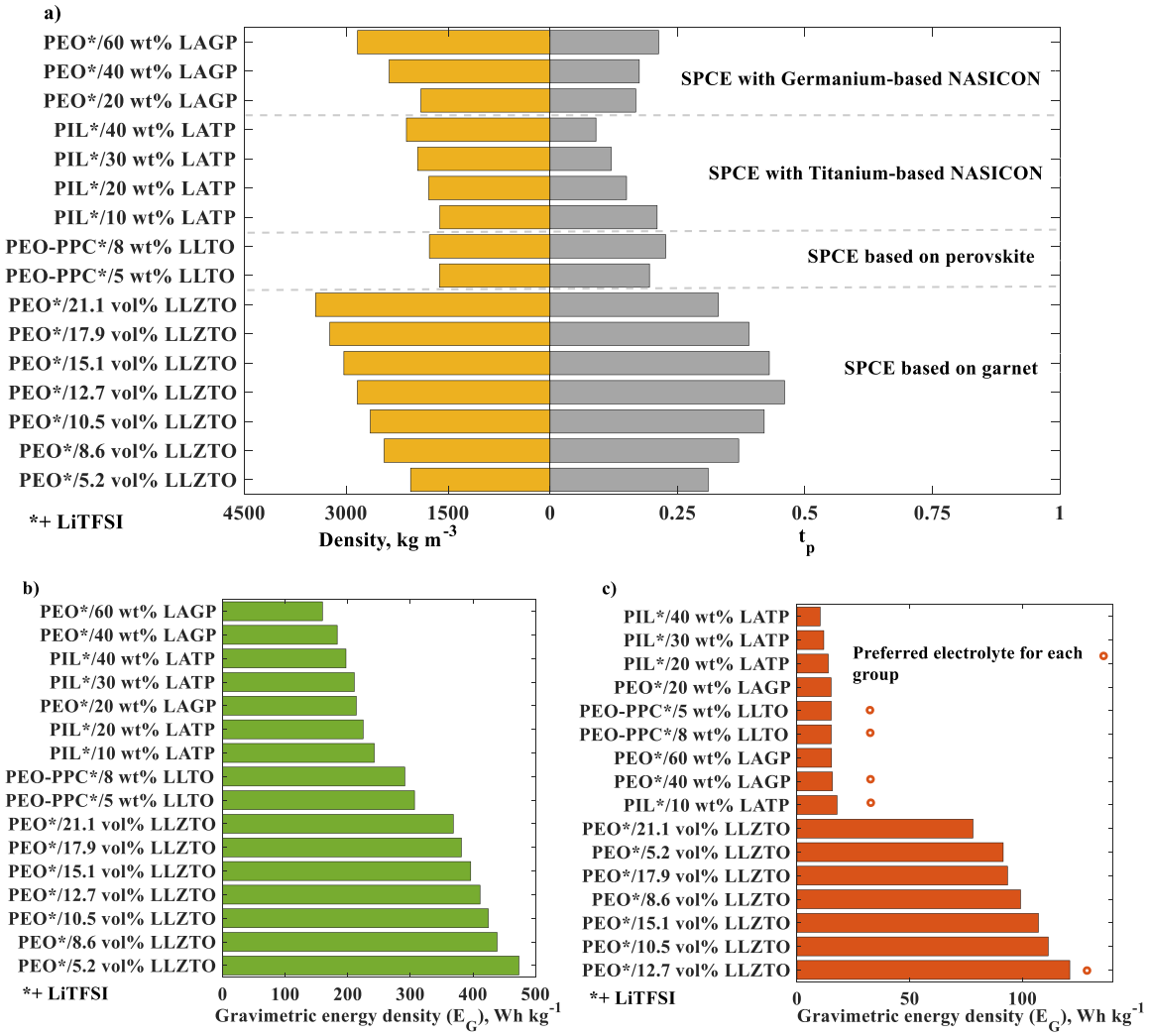

Figure 3. (a) Reported values of t_p and density of SPCE electrolytes based on Table II, (b) simulation of the impact of the various composition of SPCE electrolytes at 60 °C on the gravimetric energy density for a cell with Li metal as the anode, and NMC811 as cathode at reported SE thickness and current rates of 0.1C, and (c) 1C. Parameters according to Tables II, IV, and SI.

cells is the electrolyte type, separator thickness (which has been empirically demonstrated in the literature due to production restrictions), ionic conductivity, density, and t_p (as described in Figs. 3a and Table II).

Among SPCE with Germanium-based NASICON, those with 20 wt% and 40 wt% of LAGP show the best performance at 0.1C and 1C, respectively. The explanation is that the composite electrolyte with 40 wt% of LAGP has a higher ionic conductivity and t_p than LAGP (20 wt%), which results in ions finding a much quicker route through the electrolyte and having less diffusion limitation at an elevated discharge rate. However, due to the higher mass of oxide in the hybrid electrolyte with 40 wt% LAGP than SPCE with 20 wt% LAGP, it delivers less gravimetric energy density at a low discharge rate. SPCE with PIL-LiTFSI and a 10 wt% of LATP deliver the highest gravimetric energy density for various discharges rates in cells with titanium-based NASICON electrolyte. This may be owing to the reasons that this composition has the highest ionic conductivity and tp, as well as the lowest density of the others in the group. There is no significant difference between the gravimetric energy density of SPCE based on perovskite with PEO-PPC-LiTFSI/LLTO (8 wt%) and PEO-PPC-LiTFSI/LLTO (5 wt%) at low and high discharge rates. However, these composite electrolytes are not appropriate for operation at high current rates due to high diffusion restriction within the composite LLTO electrolyte and low t_p and ionic conductivity. Among the composite electrolyte based on garnet, the LLZTO content of 12.7 vol% results in the highest gravimetric energy density at an elevated current rate, as illustrated in Fig. 3c. Higher density of the LLZTO content (12.7 vol%) compared to the LLZTO content (5.2 vol%) leads to worse performance at lower discharge rates.

All these simulations show that, at low discharge rates, density is the most critical factor affecting gravimetric energy density. However, at an elevated discharge rate, besides density also transport relevant parameters, i.e. ionic conductivity, and t_p play a significant role in the gravimetric energy density. Since in the optimisation section, we aim to find the optimal design of the electrode for high energy applications as well as for high power and high energy application simultaneously, the best hybrid electrolyte should not have mass transfer limitation at higher discharge rates. For this reason, we selected the best electrolyte for each group, marked in red based on the results of Fig. 3c.

In the following, we compare SIC electrolytes, polymer electrolytes, and the identified best hybrid electrolyte, to select the most suitable solid electrolyte in terms of gravimetric and volumetric energy densities. In a first comparison, we consider the reported thickness of solid electrolytes, which is based on the current technology of solid-state batteries, as mentioned in Table II. In the second comparison, the modelling is performed with the same thickness of 40 μm for all solid electrolytes to answer the following question: Which kind of solid electrolyte is the most promising for the energy demand in the aviation context if the thickness can be reduced in the manufacturing step to the current thickness of garnet-based hybrid electrolytes? We expect that the reduction in thickness decreases the inactive material in the battery cell, resulting in higher gravimetric and volumetric energy densities.

Figure 4a shows the model-predicted practical gravimetric and volumetric energy densities of the cells with various solid electrolyte types and their reported thickness. As demonstrated in the figure, there is no considerable discrepancy in the gravimetric and volumetric energy densities of SIC based on LLZO, LLTO, and LLZTO at a low and elevated discharge rate. Because there is no concentration gradient in the SIC electrolyte, it can theoretically increase cell performance by allowing for a more homogeneous discharge in the electrodes and have low ohmic losses within the electrolyte even at an elevated discharge rate. LLZTO has the highest ion conductivity among the chosen SIC electrolytes. Owing to its high density of 5086 kg m^{-3},[24] LLZTO does not have the highest gravimetric energy density. The highest gravimetric energy density among SIC electrolytes is observed for LATP ones at 0.1C. However, it shows low gravimetric and volumetric energy densities due to its large separation layer. Due to the Li dendrite growth issue in these types of batteries and the necessity to avoid internal short circuits, a thick separator layer of ca. 300 μm, as shown in Fig. 4a with star points, should be employed in the construction of Li-ASSB-based on SIC electrolyte. With such high thicknesses and densities, it is impossible to attain attractive gravimetric energy densities with SIC electrolytes. A hybrid electrolyte of oxide and polymer could be a promising solution to enhance the gravimetric and volumetric energy densities of Li-based ASSB.[8–10,12,13]

Despite hybrid electrolytes of LAGP and LATP having better ionic conductivity and t_p than PEO-LiTFSI, their mixtures perform worse than polymer at elevated current rates. This is due to their higher solid electrolyte thickness of 200 μm compared to polymer electrolyte thickness of 135 μm, which results in increasing transport overpotential. The SPCE with 12.7 vol% of LLZTO has the maximum gravimetric energy density in comparison with other hybrids, SIC, and polymer electrolytes. The explanation for this is that SPCE with LLZTO can be manufactured much thinner so that less ionic overpotential is expected. They are additionally advantageous because they are more stable in contact with a lithium metal anode, and the electrochemical window of PEO-LiTFSI/LLZTO (12.7 vol%) is more than 4.7 V.[10] Hence, PEO-LiTFSI/LLZTO (12.7 vol%) could be an appropriate option to achieve a higher gravimetric density in coupling with Li and high voltage cathode materials. However, the amount of its gravimetric and volumetric energy densities are not high enough as it does not reach the 500 Wh kg^{-1} and 1000 Wh l^{-1} needed for aviation. Other hybrid electrolytes, as shown in Fig. 4a, have a higher gravimetric energy density than SIC electrolytes at low current rates, but their gravimetric and volumetric energy densities are small at a high current rate. Because of the large separator layer used to prevent internal short circuits, these electrolytes have a significant diffusion constraint at elevated discharge rates.

In practical application, the mechanical strength of solid electrolytes was shown to deteriorate if they become very thin, leading e.g. to Li dendrite growth and membrane separator fracture.[46] If these manufacturing and stability constraints can be overcome in the future, it is possible to obtain higher gravimetric and volumetric energy densities of hybrid electrolytes and SIC by reducing the electrolyte thickness, and thus the passive material and internal resistance. We want to see which electrolyte is the most promising in terms of high energy-density batteries if the thickness of all electrolytes is reduced to the same level as garnet-based hybrid electrolytes (40 μm). This model-based evaluation allows to identify those electrolyte compositions, where it is worth investing experimentally in building thinner, well-performing hybrid electrolytes. As illustrated in Fig. 4b, the gravimetric and volumetric energy densities for all solid electrolytes are significantly enhanced. Especially the SIC electrolytes have the potential to reach attractive gravimetric and volumetric energy densities if they can be produced thinner. Among the investigated SIC electrolytes, NASICON-type germanium and titanium-based have the best performance because of their lower density. Polymer-based electrolytes, in the absence of inorganic oxides-based electrolytes, could fulfil the demand of gravimetric energy density at 0.1C, but show significantly lower energy densities at 1C. However, the narrow electrochemical stability window of PEO (<3.8 V) restricts its application with high voltage cathode material like NMC811.[47] Therefore, it cannot be an appropriate solid electrolyte for the target of this study. Oxidic solid electrolytes not only are stable at these potentials, but also their mixture with PEO could enhance ion conductivity and electrochemical window stability of PEO. By mixing PEO and oxidic electrolytes, ion transport channels will be created at the interface between polymers and oxidic electrolytes, this results in further improvement of the hybrid electrolyte ionic conductivity.[13]

According to the conducted simulations, the maximum gravimetric energy density of 525 Wh kg^{-1} at 0.1C is observed for SPCE with 10 wt% of LATP. Thus, this type of solid electrolyte could be a

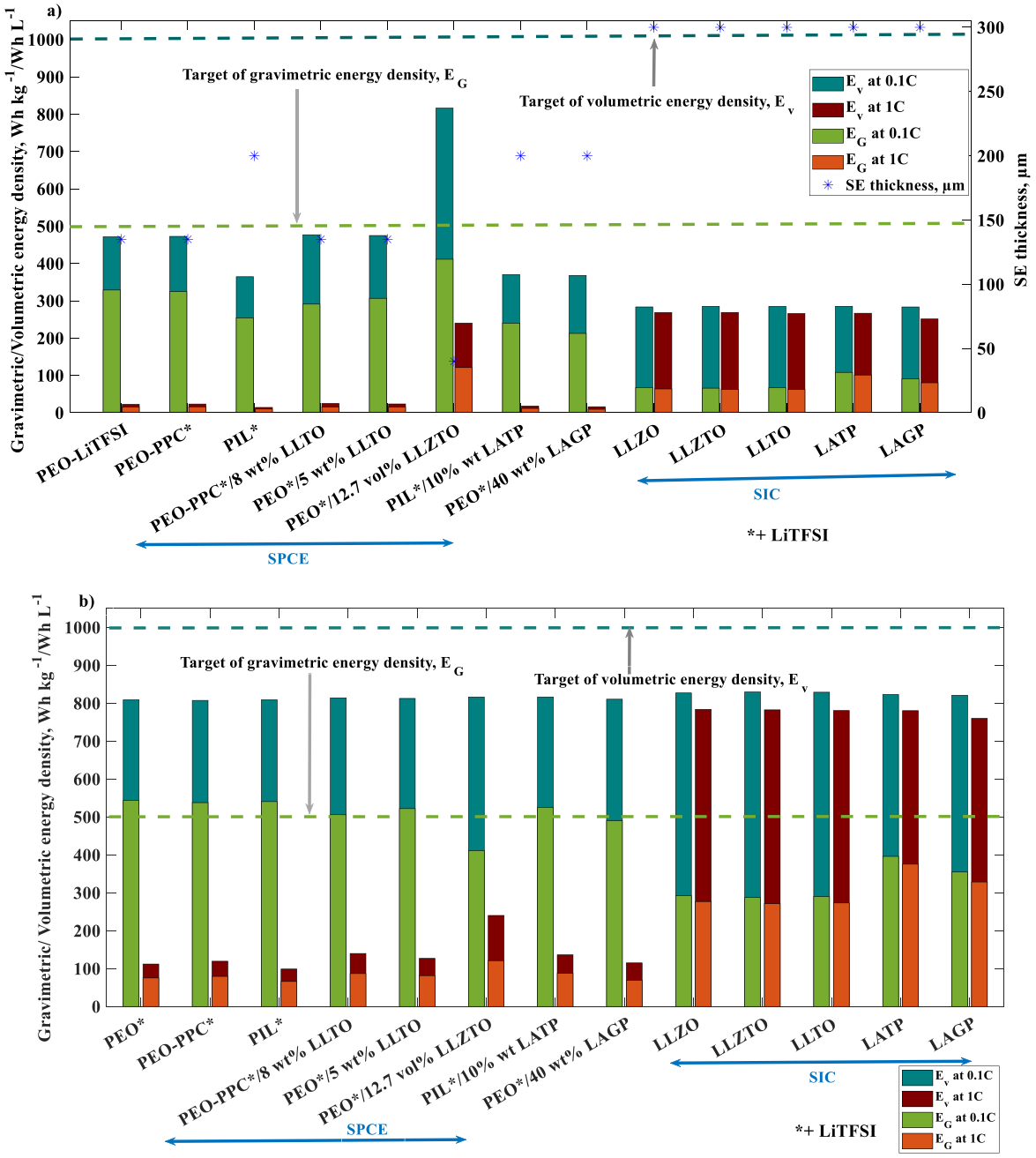

Figure 4. Comparison of SIC electrolyte, polymer, and SPCE in terms of predicted gravimetric and volumetric energy densities for a cell with Li metal as the anode, and NMC811 as cathode at (a) reported SE thickness, (b) SE thickness of 40 μm for different C-rates. Parameters according to Tables II, IV, and SI.

promising choice for future aircraft. However, its volumetric energy density and that of all other electrolytes are still not reaching the demand of 1000 Wh l^{-1}.

One way to improve gravimetric energy density is to optimise the design parameters of the battery cell. Because we aim to optimise the cell using components that are already manufacturable, a hybrid electrolyte with 12.7 vol% LLZTO, which can already now be produced in thin layers, will be employed as the solid electrolyte in the next sections. The current gravimetric energy density of such a cell is less than 500 Wh kg^{-1}, as previously noted. Therefore, in the next part, we will first perform the sensitivity analysis on the battery cell to determine which battery parameters drive the gravimetric energy density and then select decision variables for the optimisation strategy. Then we will implement a global optimisation algorithm to find an optimum design of the battery cell with 12.7 vol% LLZTO to reach the high gravimetric energy density of 500 Wh kg^{-1}.

Sensitivity analysis results.—This section aims to present sensitivity analysis and help to choose decision variables for optimising the battery towards high gravimetric energy density. As listed in Table V, the chosen input parameters of the sensitivity analysis are Li transfer number, the thickness of cathode and electrolyte, particle size of cathode material, volume fraction of cathode material, the electric conductivity of solid phase, and tortuosity. The tortuosity was estimated using Eq. 5 and its relationship with the Bruggeman factor. The gravimetric energy density is considered as the output variable. With a small sample size, the sensitivity of a parameter may be underestimated or overestimated.

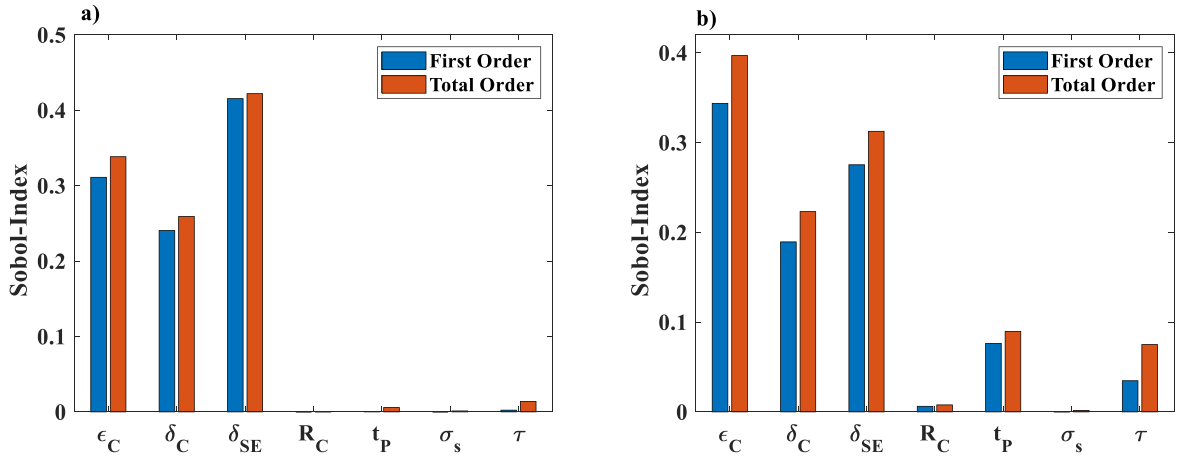

Figure 5. Comparison of the Sobol index of simulation with parameter variations for a cell with 12.7 vol% LLZTO, Li metal as the anode, and NMC811 as cathode at (a) C-rate of 0.1, (b) C-rate of 1. Parameters according to Tables II, IV, V, and SI.

Therefore, using a sufficiently large sample size to identify where the convergence of each parameter occurs is a major factor in determining sample size. As depicted in Fig. S3, a sample size of 400 stochastic parameter combinations is sufficient to get a reliable result. After a sample size of 400, the total Sobol index stabilises with minor value deviations for all variables, and convergence in the total Sobol index can be attained with each adjustment of input battery parameters. Using a sample size of 400, the influence of the input parameters on the gravimetric energy density as a model output is studied at discharge rates of 0.1C and 1C. The sensitivity analysis results for the SPCE with 12.7 vol% of LLZTO are illustrated in Fig. 5. The gravimetric energy density exhibits high sensitivities for the cathode and solid electrolyte thickness and the volume fraction of active materials in both discharge rates. Particle size and electrical conductivity are not sensitive, especially at a low current rate. t_p and tortuosity, have a considerable influence on the battery performance at elevated C-rates, due to transport limitations. Since the last two parameters are material dependent or hard to control, respectively, and we aim to optimise the cell without modifying material characteristics, they are not considered as decision variables for the optimisation model.

Despite the solid electrolyte thickness being one of the most sensitive parameters on the output response, we will not consider it as a decision parameter for the optimisation. It is evident that a higher gravimetric energy density can be reached at a thinner solid electrolyte, which we already discussed above. Thus, we assume a constant value of 40 μm, i.e. the thickness already producible for LLZTO-PEO hybrid electrolytes, as the solid electrolyte thickness, and consider the cathode thickness and volume fraction of active material as decision variables for the following simulations.

Another notable finding of sensitivity analysis is that the total Sobol indices are higher than the first order for 1C, showing that there are cross-correlations between the parameters, at higher C-rates. This means that interactions between parameters do not have the same impact as when we solely analyse the influence of individual parameters on the output. The interactions between parameters have a significant influence on gravimetric energy density. Since this interaction can only be evaluated using global sensitivity analysis and not local analysis, we recommend utilising the global technique also for the optimisation, which is already used in this study, to find an optimal electrode design more precisely.

Optimisation results.—The parameters of the initial cell design before optimisation (reference coin cell) and after optimisation are chosen such that the cell can be already manufactured based on the current technology of ASSB with potentially high performance. Thus, we choose NMC811 for the reference cell design to reach a higher gravimetric energy density. As demonstrated earlier, the hybrid electrolyte with 12.7 vol% of LLZTO has the best discharge battery performance, when taking into account present manufacturing constraints. Hence, we performed optimisation on the reference cell with this electrolyte including its typical thickness, ionic conductivity, t_p, which are based on the experiments extracted from literature, to identify those cathode parameter values, i.e., cathode thickness and volume fraction of active material, which lead to the highest gravimetric energy density for a given C-rate. The geometrical and electrochemical properties of the reference cell, such as particle size, cell geometry, Li diffusivity in the active material, the thickness of the anode and cathode electrodes, the volume fraction of active materials, and NMC811 open-circuit voltage are based on our experimental measurement. We optimised the cell for two discharge rates to identify the optimal electrode design for high-energy applications at 0.1C and high-power and high-energy applications at 1C, respectively. We also performed simulations for the optimal design of cells for 0.1C and 1C at discharge rates of 1C and 0.1C, respectively to elucidate whether the optimal proposed design for a particular application at the respective C-rate is clearly better than the reference.

Table VI presents the optimisation outcomes for these two discharge rates in comparison to the original cell design. As shown in the table, the cell with the optimal design for 0.1C shows the highest performance in terms of gravimetric and volumetric energy density in comparison to the reference cell and optimised cell for 1C, discharged at 0.1C. The cell with the optimal design for 0.1C has a significantly thicker NMC electrode of 77 μm and a higher volume fraction of active material (63%) than the reference cell and the optimised cell for 1C.

The cell with the optimal design for 1C demonstrates higher specific power and energy simultaneously in comparison to the reference cell and the optimised cell for 0.1C, discharge at 1C. The optimisation suggests a thinner cathode thickness and higher volume fraction of active materials than the reference cell to achieve high power and high energy simultaneously at 1C. These designs and their usage at 0.1C and 1C are discussed more in-depth in the following.

Even though batteries with thick electrodes can increase the proportion of active materials and thus gravimetric energy density, the full impact of the thick electrode on ASSB battery electrochemical performance should be assessed. In this regard, we analyse voltage vs specific capacity (capacity in NMC electrode) and concentration profile of Li-ions in the electrolyte within the electrode at the end of discharge over battery width for the reference cell and optimal design electrode at a given C-rate. Figure 6a shows the optimal cell with a thick electrode, which operates at 0.1C, has the largest specific capacity. As demonstrated in Fig. 6b, with increasing cathode thickness, the slope of the Li-ion concentration profile in the

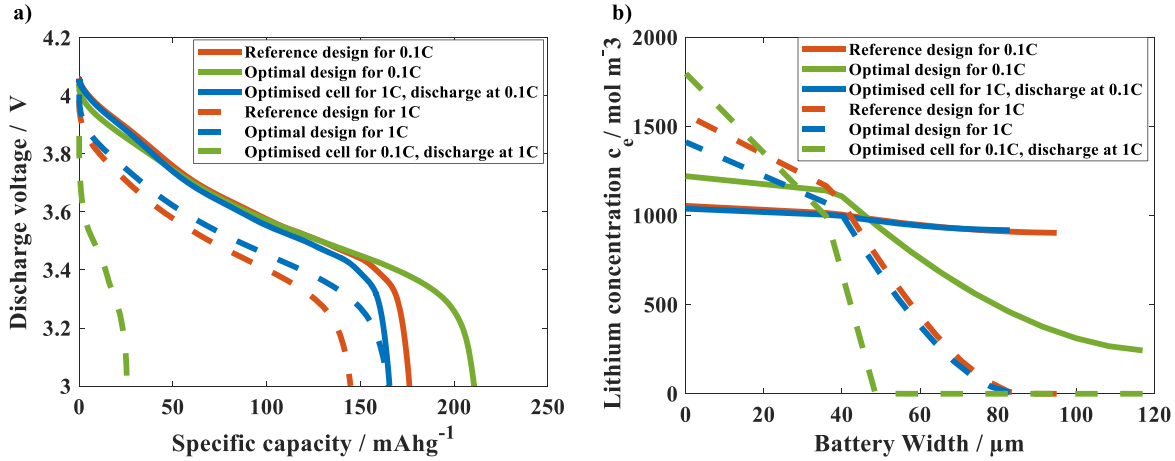

Figure 6. (a) Simulated voltage vs capacity relative to mass of NMC electrode, (b) Predicted Li-ion concentration profile within the electrolyte for the optimised Li-ion battery and the reference cell at the end of discharge at two current rates for a cell with 12.7 vol% LLZTO, Li metal as the anode, and NMC811 as the cathode. Parameters according to Tables II, IV, V, and SI.

electrolyte for the cell with the optimal design at 0.1C becomes steeper because of the longer diffusion distance; however, there is no evidence of ion starvation on the cathode side (solid green line). However, when the optimal cell for 0.1C operates at an elevated discharge rate of 1C (dashed green line), the gradient of Li-ion concentration grows larger and affects the slope of the discharge curve due to high overpotentials, resulting in decreased voltage, as visible in Fig. 6a. Although the theoretical capacity increases with increasing cathode thickness, the electrolyte overpotential overcomes the benefit of increased theoretical capacity at a higher current rate, as shown in Fig. 6a (dashed green line). As a result, the total capacity of the thick electrode cell operating at 1C is drastically reduced. The optimised cell for 1C, discharged at 0.1C, performs worse than the reference cell at 0.1C, as shown in Fig. 6a, since the cathode thickness is thinner, resulting in lower theoretical capacity. Furthermore, the gradient concentration profile in the electrolyte for these two cells does not differ much (solid blue and red lines in Fig. 6b). As a result, the theoretical capacity advantage is dominant and the reference cell at 0.1C shows a better performance than the optimised cell for 1C, discharged at 0.1C. Nevertheless, its performance in comparison to the optimised cell for 0.1C is weaker.

As shown in Fig. 6b for the cell operated and optimised at 1C, no Li-ion deficiency in the electrolyte is observed on the cathode side at the discharge of 1C based on the suggested optimal design (dashed blue line). In contrast, the Li-ion depletion at the cathode side with the reference electrode design and the optimised cell for 0.1C, discharged at 1C is obvious and leads to low C-rates as illustrated in Fig. 6a. Although the optimised cell for 0.1C, discharge at 1C can achieve a greater average power density, the cell has a severe Li-ion shortage on the cathode side. Furthermore, this cell has a gravimetric energy density of 73.66 Wh kg^{-1}, which is significantly smaller than the optimised cell for 1C (351.36 Wh kg^{-1}) and thus cannot be used for high-power, high-energy applications.

In summary, it can be stated that by model-based optimisation of the electrode design parameters, we identified the optimal cell at 0.1C with higher gravimetric and volumetric energy densities for high-energy application and the optimal electrode design at 1C for high-power and high-energy application. As shown in Table VI, at 0.1C, gravimetric and volumetric energy densities of 618 Wh kg^{-1} and 1251 Wh l^{-1}, are achieved when meeting the constraints, respectively. These values thus fulfill the mission requirement in the aviation sector, which has a volumetric and gravimetric energy density of more than 1000 Wh l^{-1} and 500 Wh kg^{-1}, respectively. We used the experimentally feasible separator layer thickness of 40 μm for the hybrid electrolyte containing 12.7 vol% LLZTO which enabled to suppress lithium dendrite growth and inhibited the cell from internal short circuits according to Ref 10. The proposed optimum cell composition therefore should be feasible to manufacture.

Conclusions

Hybrid-electric propulsion systems containing batteries have the potential to reduce overall fuel consumption and decrease weight penalties. However, in aviation, gravimetric energy density is especially important. Thus, when considering battery technology for aviation, low gravimetric energy density is a major challenge to be overcome. The oxide-based solid-state batteries, which we examined in this study, have a great potential to meet the gravimetric energy density requirements for the aviation industry. To determine the optimal electrolyte combination among oxide-based SIC and hybrid electrolytes based on PEO and oxides, we conducted a numerical analysis using mechanistic ASSB modelling. Based on available ASSB technology, SIC electrolytes cannot achieve a higher gravimetric energy density than hybrid electrolytes at low current rates due to their high density. It was also found that the best electrolyte in terms of gravimetric energy density based on currently available materials is SPCE with 12.7 vol% of LLZTO. However, SPCE with 10 wt% of LATP is suggested as a promising solid electrolyte for future aircraft if researchers succeed to decrease its electrolyte thickness and chemical stability in contact with lithium metal anode. Further, sensitivity analyses enabled us to identify the impact of battery parameters and cell design on the gravimetric energy density. The cathode thickness and volume fraction of cathode materials were determined as critical parameters for increasing the gravimetric energy density. Furthermore, we applied an evolutionary algorithm to optimise gravimetric energy density by changing these two electrode design parameters. After optimisation, gravimetric and volumetric energy densities of 618 Wh kg^{-1} and 1251 Wh l^{-1} for 0.1C discharge are achieved, respectively, indicating that the cell with the optimal electrode design could meet the mission demand in the aviation industry with a gravimetric energy density of 500 Wh kg^{-1} and volumetric energy density of 1000 Wh l^{-1}.

In conclusion, the findings of this study reveal that our physics-based modelling in conjunction with an optimisation algorithm predicts the optimal composition of ASSB for a given constraint and thus supports the time- and cost-effective development of batteries that fulfil mission requirements, e.g. in the aviation sector. Similarly, as for Li-ion batteries,[34] we found that optimal designs strongly depend on the concrete objective (here: 0.1C operation), and it should be carefully checked if they are able to meet further constraints, e.g. sufficient gravimetric energy density at 1C operation. Where necessary, additional constraints or multi-objective

optimisation may be conducted to meet all constraints. ASSB model-based optimisation can accurately design batteries not only for the respective C-rate but also could find optimal electrode design of battery based on the mission profile. From an experimental point of view for the future and based on the performed simulation, a multilayer solid electrolyte, which combines the advantages of two different electrolytes could allow to improve the gravimetric energy density of ASSB further.

Acknowledgment

We would like to acknowledge the funding of the European Union's Horizon 2020 research and innovation program under grant agreement No 875006 IMOTHEP and Deutsche Forschungsgemeinschaft (DFG, German Research Foundation) under Germany's Excellence Strategy –EXC 2163/1-Sustainable and Energy Efficient Aviation –Project-ID 390881007.

ORCID

Florian Baakes https://orcid.org/0000-0001-6876-0020
Ulrike Krewer https://orcid.org/0000-0002-5984-5935

References

1. M. Tariq, A. I. Maswood, C. J. Gajanayake, and A. K. Gupta, *IECON Proc. (Industrial Electron. Conf. 4429* (2016).
2. J. Hoelzen, Y. Liu, B. Bensmann, C. Winnefeld, A. Elham, J. Friedrichs, and R. Hanke-Rauschenbach, *Energies*, **11**, 1 (2018).
3. S. Chen, J. Zhang, L. Nie, X. Hu, Y. Huang, Y. Yu, and W. Liu, *Adv. Mater.*, **33**, 1 (2021).
4. Z. Deng, X. Hu, S. Member, X. Lin, L. Xu, and J. Li, *IEEE Transactions on Transportation Electrification*, **7782**, 464 (2020).
5. D. Karabelli, K. P. Birke, and M. Weeber, *Batteries*, **7**, 18 (2021).
6. M. V. Reddy, C. M. Julien, A. Mauger, and K. Zaghib, *Nanomaterials*, **10**, 1 (2020).
7. Q. Zhou, Q. Li, S. Liu, X. Yin, B. Huang, and M. Sheng, *J. Power Sources*, **482**, 228929 (2021).
8. L. Zhu, P. Zhu, Q. Fang, M. Jing, X. Shen, and L. Yang, *Electrochim. Acta*, **292**, 718 (2018).
9. F. Ma, Z. Zhang, W. Yan, X. Ma, D. Sun, Y. Jin, X. Chen, and K. He, *ACS Sustain. Chem. Eng.*, **7**, 4675 (2019).
10. J. Zhang, N. Zhao, M. Zhang, Y. Li, P. K. Chu, X. Guo, Z. Di, X. Wang, and H. Li, *Nano Energy*, **28**, 447 (2016).
11. S. Chen, J. Zhang, L. Nie, X. Hu, Y. Huang, Y. Yu, and W. Liu, *Adv. Mater.*, **33**, 1 (2021).
12. G. Piana, F. Bella, F. Geobaldo, G. Meligrana, and C. Gerbaldi, *J. Energy Storage*, **26**, 100947 (2019).
13. L. Zhu et al., *Int. J. Energy Res.*, **43**, 4854 (2019).
14. O. Kramer, *Genet. Algorithm Essentials* (Springer, Berlin) 11 (2017).
15. V. Laue, F. Röder, and U. Krewer, *J. Appl. Electrochem.*, **51**, 1253 (2021).
16. N. Lin, X. Xie, R. Schenkendorf, and U. Krewer, *J. Electrochem. Soc.*, **165**, A1169 (2018).
17. K. Becker-Steinberger, S. Funken, M. Landstorfer, and K. Urban, *E. C. S. Transactions*, **25**, 285 (2010).
18. N. Wolff, F. Röder, and U. Krewer, *Electrochim. Acta*, **284**, 639 (2018).
19. D. Danilov, R. A. H. Niessen, and P. H. L. Notten, *J. Electrochem. Soc.*, **158**, A215 (2011).
20. V. Laue, N. Wolff, F. Röder, and U. Krewer, *Energy Technology*, **1801049**, 1 (2020).
21. V. Laue, F. Röder, and U. Krewer, *Elsevier Ltd.*, **314**, 20 (2019).
22. U. Krewer, F. Röder, E. Harinath, R. D. Braatz, B. Bedürftig, and R. Findeisen, *J. Electrochem. Soc.*, **165**, A3656 (2018).
23. A. Jokar, B. Rajabloo, M. Désilets, and M. Lacroix, *J. Power Sources*, **327**, 44 (2016).
24. Y. Meesala, Y.-K. Liao, A. Jena, N.-H. Yang, W. K. Pang, S.-F. Hu, H. Chang, C.-E. Liu, S.-C. Liao, and J.-M. Chen, *J. Mater. Chem. A*, **7**, 8589 (2019).
25. Z. Zhang et al., *Energy Environ. Sci.*, **11**, 1945 (2018).
26. W. Zhao, J. Yi, P. He, and H. Zhou, *Solid-State Electrolytes for Lithium-Ion Batteries: Fundamentals, Challenges and Perspectives* (Springer, Berlin) (2019).
27. K. Waetzig, A. Rost, C. Heubner, M. Coeler, K. Nikolowski, M. Wolter, and J. Schilm, *J. Alloys Compd.*, **818**, 153237 (2020).
28. S. Wang, Y. Ding, G. Zhou, G. Yu, and A. Manthiram, *ACS Energy Lett.*, **1**, 1080 (2016).
29. L. Fan, S. Wei, S. Li, Q. Li, and Y. Lu, *Adv. Energy Mater.*, **8**, 1 (2018).
30. J. Schmalstieg, C. Rahe, M. Ecker, and D. U. Sauer, *J. Electrochem. Soc.*, **165**, A3799 (2018).
31. G. Lenze, V. Laue, and U. Krewer, *J. Electrochem. Soc.*, **166**, A2950 (2019).
32. J. Sturm, S. Ludwig, J. Zwirner, C. Ramirez-Garcia, B. Heinrich, M. F. Horsche, and A. Jossen, *J. Power Sources*, **436**, 226834 (2019).
33. X. Ban, W. Zhang, N. Chen, and C. Sun, *J. Phys. Chem. C*, **122**, 9852 (2018).
34. D. Witt, D. Wilde, F. Baakes, F. Belkhir, F. Röder, and U. Krewer, *Energy Technol.*, **9**, 2000989 (2021).
35. E. Hosseinzadeh, J. Marco, and P. Jennings, *Energies*, **10**, 1278 (2017).
36. I. Sobol, "Sensitivity estimates for nonlinear mathematical models." *Mater. Model.*, **2**, 112 (1990).
37. V. Triantafyllidiis, W. W. Xing, P. K. Leung, A. Rodchanarowan, and A. A. Shah, *J. Phys. Conf. Ser.*, **1039** (2018).
38. M. Quarti and W. G. Bessler, *Energy Technol.*, **9**, 2001122 (2021).
39. C.-H. Chen, F. Brosa Planella, K. O'Regan, D. Gastol, W. D. Widanage, and E. Kendrick, *J. Electrochem. Soc.*, **167**, 080534 (2020).
40. A. Bielefeld, D. A. Weber, and J. Janek, *J. Phys. Chem. C*, **123**, 1626 (2019).
41. R. Tian, N. Alcala, S. J. K. O'Neill, D. V. Horvath, J. Coelho, A. J. Griffin, Y. Zhang, V. Nicolosi, C. O'Dwyer, and J. N. Coleman, *ACS Appl. Energy Mater.*, **3**, 2966 (2020).
42. N. Xue, W. Du, A. Gupta, W. Shyy, A. M. Sastry, and J. R. R. A. Martins, *J. Electrochem. Soc.*, **160**, A1071 (2013).
43. G. Merei, C. Berger, and D. U. Sauer, *Sol. Energy*, **97**, 460 (2013).
44. Z. Chen, C. C. Mi, Y. Fu, J. Xu, and X. Gong, *J. Power Sources*, **240**, 184 (2013).
45. X. Ren et al., *Joule*, **3**, 1662 (2019).
46. J. Wu, L. Yuan, W. Zhang, Z. Li, X. Xie, and Y. Huang, *Energy Environ. Sci.*, **14**, 12 (2021).
47. S. N. Patel, *ACS Macro Lett.*, **10**, 141 (2021).